Analysis of the Heat Index in the Mesoamerica and Caribbean Region

Nazario D. Ramirez-Beltran,[a] Jorge E. Gonzalez,[b] Joan M. Castro,[c] Moises Angeles,[b]
Eric W. Harmsen,[d] and Cesar M. Salazar[a]

[a] *Department of Industrial Engineering, University of Puerto Rico, Mayagüez, Puerto Rico*
[b] *Department of Mechanical Engineering, City College of New York, New York, New York*
[c] *Department of Civil Engineering, University of Puerto Rico, Mayagüez, Puerto Rico*
[d] *Department of Agricultural and Biosystems Engineering, University of Puerto Rico, Mayagüez, Puerto Rico*

ABSTRACT

Hourly data collected from ground stations were used to study the maximum daytime heat index H_i in the Mesoamerica and Caribbean Sea (MAC) region for a 35-yr period (1980–2014). Observations of H_i revealed larger values during the rainy season and smaller values during the dry season. The H_i climatology exhibits the largest values in Mesoamerica, followed by the Greater Antilles and then by the Lesser Antilles. The trend in H_i indicates a notable increasing pattern of $0.05°C\,yr^{-1}$ ($0.10°F\,yr^{-1}$), and the trends are more prominent in Mesoamerica than in Caribbean countries. This work also includes the analysis of heat index extreme events (HIEE). Usually the extreme values of the heat index are used for advising heat warning events, and it was found that 45 HIEEs occurred during the studied period. The average duration of HIEE was 2.4 days, and the average relative intensity (excess over the threshold) was $2.4°C$ ($4.3°F$). It was found that 82% of HIEE lasted 2 or 2.5 days and 80% exhibited relative intensity of $3°C$ ($5.4°F$) or less. It was also found that the frequency of extreme events has intensified since 1991, with the highest incidences occurring in 1995, 1998, 2005 and 2010, and these years coincide with the cool phase of El Niño–Southern Oscillation (ENSO). Therefore, the occurrences of HIEE in the MAC region appear to be at least partially influenced by ENSO episodes.

1. Introduction

The heat index is the combination of the air temperature and relative humidity (RH) and is an attempt to estimate what humans feel as an apparent temperature. Variations in the heat index are linked to both human health and energy demands to maintain indoor room comfort (González-Cruz et al. 2013) and hence it is important to characterize the behavior of the heat index. This index is based on the human energy balance and was determined as the result of various extensive biometeorological studies (Fanger 1970; Steadman 1979; Rothfusz 1990). The human body usually adapts to hot temperatures by perspiration, when heat is removed from our body by sweat evaporation. High values of RH

reduce the evaporation rate, causing lower heat removal from our body and hence the sensation of being overheated. Steadman (1979) studied the human response under different environmental conditions to derive a theory for estimating the apparent temperature or heat index. His method takes into account the effects of air temperature and RH on the reaction of the human body and expresses the physiological reaction, clothing resistance, moisture content, and heat-transfer interactions as an apparent temperature. Steadman's work was based on the human biometeorology study conducted by Fanger (1970), who measured the reaction of 256 adults wearing different clothing and performing various physical activities under certain environmental conditions. Fanger's experiments provided the basis for deriving physiological data describing the average heat and moisture transfer. Steadman (1979) derived a method for estimating the apparent temperature based on the amount of heat lost via exhaling and the skin's resistance to heat and moisture transfer. Rothfusz (1990) used Steadman's results to develop a regression equation,

which expresses the relationship between temperatures at different RHs and the skin's resistance to heat and moisture transfer. The National Weather Service (NWS) developed its own algorithm for estimating the heat index based on Steadman's and Rothfusz's work. This method was adopted and it is available online (NWS 2016), with a detailed description of the algorithm given by Anderson et al. (2013).

Dixon (1998) reported the heat index climatological conditions in the southern United States, and pointed out that the climatological conditions can be used to evaluate the forecasted heat index severity and assisting with the issuance of hazardous heat advisories. It is known when the heat index is greater than or equal to 40.5°C (105°F) the warmer environment is dangerous and can potentially cause heat cramps and heat stroke when exposure is prolonged in combination with physical activity (NWS 2017). Dixon (1998) reported on 10 yr (1980–89) of summertime daily air temperature and RH data for 40 stations. New Orleans, Louisiana, recorded the largest heat index: 51.1°C (124°F). Rakib (2013) presented the temporal variation of extreme temperatures in Bangladesh. The variables considered in this study include the average seasonal maximum and minimum air temperature, RH, and maximum heat index. Daily records were obtained from 18 meteorological stations during the period (1981–2010). Rakib (2013) observed a significant increase in air temperature during the past decades, especially along the coastal and central areas of Bangladesh. A larger maximum heat index was also observed during the wet season.

The NWS issues an "excessive heat warning" (NWS 2017) when the maximum heat index temperature is expected to be 40.6°C (105°F) or higher for at least 2 days and the nighttime air temperatures will not drop below 21.1°C (75°F). However, these criteria vary across the country, especially for areas not accustomed to extreme heat conditions. Robinson (2001) suggested that heat watches and warnings are issued when the heat index is greater than or equal to 40.6°C (105°F) during the daytime and greater than or equal to 26.6°C (80°F) at nighttime for at least two consecutive days. Thus, the heat index extreme event (HIEE) can be used to anticipate the potential occurrence of a heat wave.

A heat wave is a persistent period of having a significant temperature deviation from the normal climate conditions of a given region, and consequently a heat wave can occur in a region with either a hot, warm, or cold climate. In general, every location has its own and unique climatology of heat, and consequently, there are several definitions of heat waves, but all of them include some notions of persistent extreme high temperatures.

The World Meteorological Organization defines a heat wave as the event when the daily maximum temperature exceeds the average maximum temperature by 5°C (9°F) for more than five consecutive days, where the normal period is from 1961 to 1990 (MetOffice 2015). In the United States a heat wave is defined as a period of at least two consecutive days of excessively hot weather (American Meteorological Society 2015). In the northeast, which is characterized by having high humidity, a heat wave is three consecutive days where temperatures reach or exceed 32.2°C (90°F). In dry zones, the heat wave occurs when the temperature reaches 37.8°C (100°F) for three or more consecutive days. The HIEE is a different phenomenon from the heat wave, since the heat wave requires persistent high temperatures, whereas the HIEE requires persistent high temperatures, which are combined with observed RH values.

To the authors' knowledge, there are no published scientific studies of a heat index over the MAC region; however, studies do show that extreme episodes of the heat index are triggering serious public health issues in most midlatitude and continental cities (Wang et al. 2012; Loughnan et al. 2014; Méndez-Lázaro et al. 2015; Portier et al. 2010). Therefore, this paper focuses on understanding the climatology and trends of H_i, as well as analyzing the extreme events in terms of duration, intensity, and frequency in the MAC region. Section 2 of this paper explains what types of data were used. Section 3 describes the methodology, which includes the major challenges encountered when dealing with weather station data; a general overview of the MAC climate characteristics; the analyses of H_i; and the characterization of HIEE. Section 4 presents an analysis of our results, which are organized into three parts: station characteristics, H_i trends and climatology, and analysis of extreme events. Section 5 includes a summary of the work and our conclusions.

2. Data

Two types of data were used in this research: reanalysis data and observations from weather stations. The source of the first type of data was the National Centers for Environmental Prediction–National Center for Atmospheric Research (NCEP–NCAR) reanalysis. Thirty-five years (1980–2014) of 6-hourly data were used for estimating the MAC climate characteristics and are used to describe the spatial variability of the regional H_i pattern (NCEP 2016a). The NCEP–NCAR reanalysis dataset includes the following domain over 0°–30°N and 60°–100°W, which corresponds to (13 × 18) 234 grids with 2.5° × 2.5° resolution. NCEP–NCAR

reanalysis data are developed by using a state-of-the-art analysis/forecast system to perform data assimilation using past global data from 1948 to the present. Thus, there are systematic differences between the NCEP–NCAR reanalysis and observational datasets (NCEP 2016b). For a given grid, the NCEP–NCAR data represent the average value for a relatively large area of a specific variable, whereas a station observation is a measurement of a single point. Hence, temperatures and RH from NCEP–NCAR reanalysis data are expected to be different from station measurements. However, NCEP–NCAR data simplify calculations, since there are no missing values, and provide the opportunity to derive insights about the behavior of meteorological variables.

Thirty-five years' (1980–2014) of hourly data from 15 ground stations were also used to perform H_i analyses. The source for the weather station data is the National Center for Environmental Information (NCEI 2016), which also includes the Global Historical Climatology Network (GHCN). The MAC region station data are mostly limited by the availability of observations of dewpoint temperature over 35 yr. The characteristics of the Caribbean and Mesoamerica stations, along with the percentage of data for each station, are given in Table 1, which also includes the original and filtered data, after applying data quality control. The MAC region (5°–30°N and 90°–60°W) includes the Caribbean Sea, which is divided into the Lesser and Greater Antilles, and Mesoamerica, which includes parts of Mexico, Central America, and the northern part of South America, as shown in Fig. 1.

3. Methodology

The methodology applied in this research includes five major tasks designed to develop a strategy for accomplishing the objectives of this work: 1) evaluate the quality of the weather station data, 2) use NCEP–NCAR data to obtain climate characteristics of the MAC region, 3) present the heat index definition and its 24-h climatology, 4) describe the techniques for computing trends and climatology patterns of H_i, and 5) describe the analysis of the HIEE.

a. Data quality control

Ground station data recorded the real and inherent patterns of behavior of the atmosphere and revealed the actual climate patterns and variability. However, working with long-term ground station records is challenging since each individual station is accompanied by their own set of inherited obstacles. For example, the types of instruments used vary since they belong to

different countries. The observations were collected at different frequencies: every 1, 3, or 6 h. It should be noted that the frequency of data collection affects the accuracy on the calculation of H_i. Observations during the daytime are more abundant than during the nighttime. Some stations show inconsistencies in the frequency of data collection.

A homogeneous climate time series is defined as one where variations are caused only by alterations in weather and climate (Peterson et al. 1998a). Thus, inhomogeneous climate data include errors such as drifts, jumps, and changes in variability. These types of error are associated with instrument changes, noncalibration, station moves, urbanization, different observation times, human errors, etc. The inhomogeneities can bias a time series and lead to misinterpretations of the studied climate (Peterson et al. 1998b). There are several algorithms and strategies that help in detecting and fixing the inhomogeneity features in the climate data (Alexandersson 1986; Peterson et al. 1998a,b; Reeves et al. 2007; Gallagher et al. 2013; Menne et al. 2009).

A request for information regarding the location and equipment history of the studied stations was submitted; however, no information corresponding to the NCEI stations was found. The available statistical tools usually work with a station, which is surrounded by similar stations, and the available observations from the nearby stations are used to remove the inhomogeneities of the station in question (Peterson et al. 1998a,b; Reeves et al. 2007). Air and dewpoint temperatures were collected from weather stations, which are mostly located at international airports. Because of the long-term duration of these data, several of the datasets contained inhomogeneities. The stations that provided the required data for this study are isolated weather stations, and, consequently, conventional tools are not applicable for treating inhomogeneous time series. However, an alternative method was developed in this work and consists of removing values that are not likely to belong to a given climate dataset. Thus, the implemented approach for each station includes five steps.

1) REMOVAL OF INSUFFICIENT DATA

Data were organized for each hour, and 24 time series were created. One series was created with daily observations at 0000 UTC, the second series at 0100 UTC, etc., until completing the 24th time series at 2300 UTC. These series are called hour-daily (HD) time series, and each complete time series includes 12 784 HD observations. Therefore, any HD time series that has more than 75% missing values was removed from the dataset, because of a lack of sufficient data to be analyzed.

TABLE 1. Characteristics of the MAC stations.

Station name and location	Lat (°N)	Lon (°W)	Elev (m)	Original data (No. of days)	Filtered data (No. of days)	Avg air temperature T_{max} (°C)	Avg RH (%)	Avg H_i (°C)	Diff $H_i - T_{max}$ (°C)
Robert L. Bradshaw International Airport, Basseville, St. Kitts and Nevis	17.311	62.719	51.8	95% (12 101)	93% (11 888)	29.3	68.5	33.4	4.1
V. C. Bird International Airport, St. John's, Antigua and Barbuda	17.137	61.793	18.9	95% (12 203)	94% (12 025)	29.4	67.4	33.2	3.8
Pointe-à-Pitre Le Raizet Airport, Pointe-à-Pitre, Guadeloupe	16.265	61.532	11	71% (9068)	67% (8584)	29	69.8	32.8	3.8
Martinique Aimé Césaire International Airport, Le Lamentin, Martinique	14.591	61.003	4.9	90% (11 509)	89% (11 341)	29.9	66.2	33.9	4
E. T. Joshua Airport, Kingstown, St. Vincent	13.144	61.211	20.1	85% (10 920)	84% (10 754)	29.7	68.6	34	4.3
Luis Muñoz Marín International Airport, San Juan, Puerto Rico	18.417	66.000	4	99% (12 630)	97% (12 454)	29.7	64.8	33.4	3.7
Cibao International Airport, Santiago de los Caballeros, Dominican Republic	19.406	70.605	172.2	89% (11 441)	87% (11 189)	30.4	57.9	33.2	2.8
Sangster International Airport, Montego Bay, Jamaica	18.504	77.913	1.2	99% (12 627)	94% (12 052)	30.1	68.1	35	4.9
Toussaint Louverture International Airport, Port-au-Prince, Haiti	18.580	72.293	37.2	80% (10 245)	73% (9305)	32	51.4	34.8	2.8
Golosón International Airport, La Ceiba, Honduras	15.742	86.853	14.9	95% (12 150)	87% (11 116)	29.5	69.6	34.1	4.6
Jose Marti International Airport, Havana, Cuba	22.989	82.409	64	97% (12 391)	95% (12 132)	29.2	60.3	32.1	2.9
Miami International Airport, Miami, Florida	25.791	80.316	8.8	99% (12 695)	97% (12 382)	28.6	57.3	31	2.4
La Chinita International Airport, Maracaibo, Venezuela	10.558	71.728	71.6	92% (11 768)	89% (11 437)	32.8	58.1	38.3	5.5
Ernesto Cortissoz International Airport, Soledad, Colombia	10.890	74.781	29.9	99% (12 669)	95% (12 224)	31.7	65	37.9	6.2
Valladolid Airport, Villanubla, Mexico	20.683	88.200	27	90% (11 513)	88% (11 344)	30.7	62	35.1	4.4

2) REMOVAL OF HOURLY INCONSISTENT DATA

An inconsistent value is defined as a value that is not likely to belong to the majority of the values of a given climate dataset. One approach for detecting inconsistent data is to use Chebyshev's inequality (Rohatgi 1976). The advantage of using Chebyshev's inequality is that it is a robust approach for detecting inconsistent data and does not require knowledge of the probability distribution of the underlying climate data. Chebyshev's inequality can be expressed as follows:

$$P(|x_i - \mu_i| > k\sigma_i) \le 1/k^2, \qquad (1)$$

where P is the probability statement; μ_i and σ_i are the mean and standard deviation, respectively, of the

climate data x_i (air or dewpoint temperatures) at the ith station; and $k > 1$. As a result, any value that falls outside this interval ($\mu_i \pm k\sigma_i$) is unlikely to be a real observation and will be declared an inconsistent record. Any value satisfying the aforementioned condition was removed from the dataset. Thus, an inconsistent value may be detected by using a k value between 3 and 5. A k value of 3 was selected since it provided satisfactory results. As the value of k is reduced, the screening procedure becomes more restrictive. Chebyshev's probability statement indicates that, for a k value of three, 89% or more of the selected data are likely to correspond to the actual observed climate data. The mean and standard deviation for each HD time series were estimated using the total number of available observations for the underlying time series. Inconsistent data
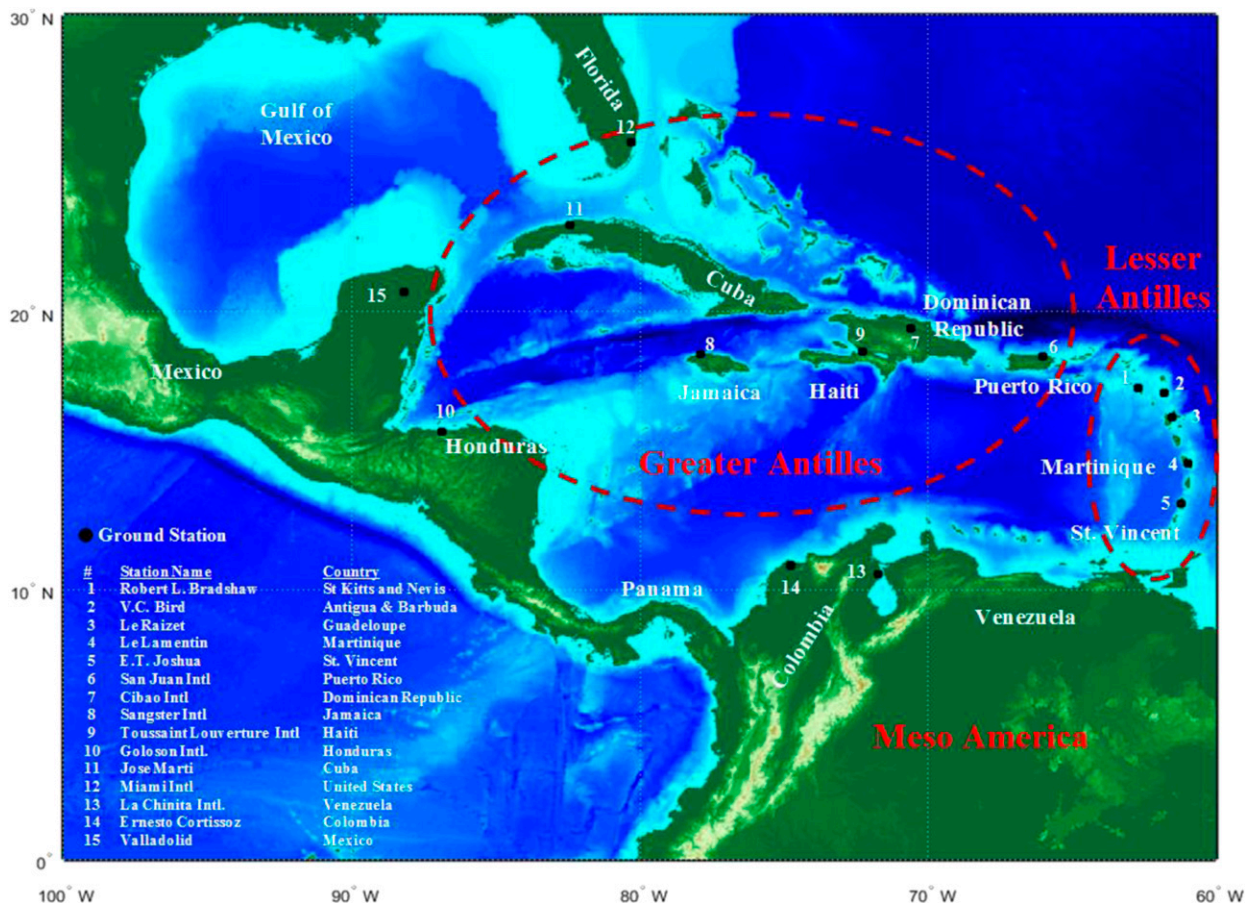
FIG. 1. Location of the MAC region. The numbers indicate the names and locations of the selected stations, and the red dashes indicate the homogeneous regions associated with the Greater and Lesser Antilles.

were considered to be missing values and were not estimated in order to avoid deriving fictitious results and incorrect conclusions.

3) REMOVAL OF 24-H INCONSISTENT DATA

The third rule consists of removing any value where the difference in temperature for the preceding or following day was greater than 25°C (77°F). Hence, searching for inconsistent data was computed by using $|x_t - x_{t-1}| > 25°C$ (77°F), where t is the corresponding time index for the HD time series.

4) REMOVAL OF JULIAN DAY INCONSISTENT DATA

The data were organized as follows. First, we selected the observed value at 0000 UTC from the first Julian day (i.e., yearday) and from 1980. Second, we selected the observed value at 0000 UTC from the first Julian day and from 1981, and repeated the process until collecting the last observation at 0000 UTC from the first Julian day and from 2014. At this stage, the

first of 35 observations are completed. The second series was created by repeating the previous steps but by using the second Julian day. Thus, the last series at 0000 UTC will be created by repeating the previous steps and using the 365th Julian day. The process is then repeated at 0100 UTC to create another 365 series, with each one having 35 observations. The previous steps are repeated again at 0200 UTC and so on, until completing the last series at 2300 UTC. These series are defined as Hour–Julian day (HJ) time series. Chebyshev's inequality was used to detect inconsistent values in each series, and the mean and standard deviation were computed for each of the HJ time series.

5) FINAL ELIMINATION OF INCONSISTENT DATA

The hourly data were reorganized in the original format and Chebyshev's inequality was again used to remove inconsistent data. The average and standard deviation were computed using all of the filtered

data. Table 1 shows the percentage of original and the filtered data, and Fig. 2 shows the original and the filtered data for stations located in Antigua and Barbuda, Cuba, and Venezuela. These stations represent examples for the Lesser and Greater Antilles, and Mesoamerica, respectively. Figure 2 shows that values that are not likely to belong to real observations were subsequently and successfully removed using Chebyshev's inequality.

b. Mesoamerica and Caribbean climate characteristics

The MAC region receives intense solar irradiance every day because of its proximity to Earth's equator. The climatology analyses in this section are based on daily averages of 6-hourly data extracted from the NCEP–NCAR dataset during the studied period. In this section, H_i was computed using the maximum of the 6-hourly data of air temperature and the corresponding RH. The average over the entire period and the annual trend were computed for every grid.

The climatology of air temperature follows a unimodal distribution receiving the largest air temperature in August and the smallest in January (Fig. 3a). The H_i climatology follows a similar pattern of daily maximum air temperature T_{max} and is given in Fig. 3b. The climatology of the RH follows a bimodal distribution and starts ascending in March until it reaches its peak in June, with a second, smaller peak occurring during September–October, and then descending until completing the cycle in March (Fig. 3c). This follows the reported rainfall bimodal climatology for the Caribbean (Angeles et al. 2010) and the observed RH. The rainfall increases humidity during the rainy season and decreases it during the dry season. The ocean increases the RH as a result of evaporation and moisture advection, which brings considerable humidity to the MAC region. The average spatial distribution shows that temperatures reach their largest values over the ocean and the RH shows the largest values over the Mesoamerican region (Figs. 3d,f). The spatial distribution of averages and trends of H_i were computed and are exhibited in Figs. 3e and 3g, respectively. The largest H_i values over the land area are observed in Mexico (Yucatan Peninsula), Cuba, Haiti, Jamaica, and Puerto Rico. On the other hand, the largest increasing trends in H_i over land areas are exhibited in the Lesser Antilles followed by the Greater Antilles.

Precipitation is primarily affected by troughs embedded in easterly waves during the rainy season (May–October), generating large amounts of rainfall in the Caribbean basin. In addition, subsidence from Central America, the Southern Oscillation by means of vertical wind shear, wind divergence, the North Atlantic Oscillation, and Saharan dust all contribute to the day-to-day rainfall variations (Goldenberg et al. 2001; Giannini et al. 2001; Jury 2015). Cold fronts generate large cloudy areas and precipitation during winter months. The confluence of these synoptic-scale events causes the Caribbean rainy season to follow a bimodal distribution (Angeles et al. 2010), dividing the season into an early rainfall period (May–July) and a late rainfall period (August–October), with a short drought period in July. The first rainfall peak occurs in May and the second in September. The lowest amount of precipitation in the Caribbean occurs from December to March and is known as the dry season.

c. Estimation of the heat index and 24-h climatology

Robinson (2001) defines the heat index as the combination of the ambient temperature and RH that approximates the environmental aspect of the thermal regime of a human body. There are several methods for estimating the heat index. Anderson et al. (2013) investigated the performance of 21 different algorithms under U.S. weather conditions. They used daily 2011 weather data, including mean air temperature, mean dewpoint temperature, and mean RH, in all 50 U.S. state capitals. They analyzed whether each algorithm produced heat index values consistent with Steadman's original apparent temperature (Steadman 1979) and found that the algorithms were inconsistent across studies. They concluded that the NWS algorithm provides reproducible and consistent environmental results. In this work, we adopted the NWS approach described in Anderson et al. (2013).

Typically, temperature and RH are combined to develop short-term heat index forecasts with the goal of providing heat warnings to the public. The approach used in this work is different from the standard use of the heat index, in the sense that we are using information from a station to calculate the heat index, and climatology and trends are based on 35 yr of hourly data. However, we adopted the standard algorithm to calculate the heat index (NWS 2016; Anderson et al. 2013).

Usually, stations reported hourly data during the daytime, and consequently H_i at a given station was calculated using the maximum of the hourly air temperature recorded during the hours from 1000 to 2200 UTC, and the dewpoint was selected at the
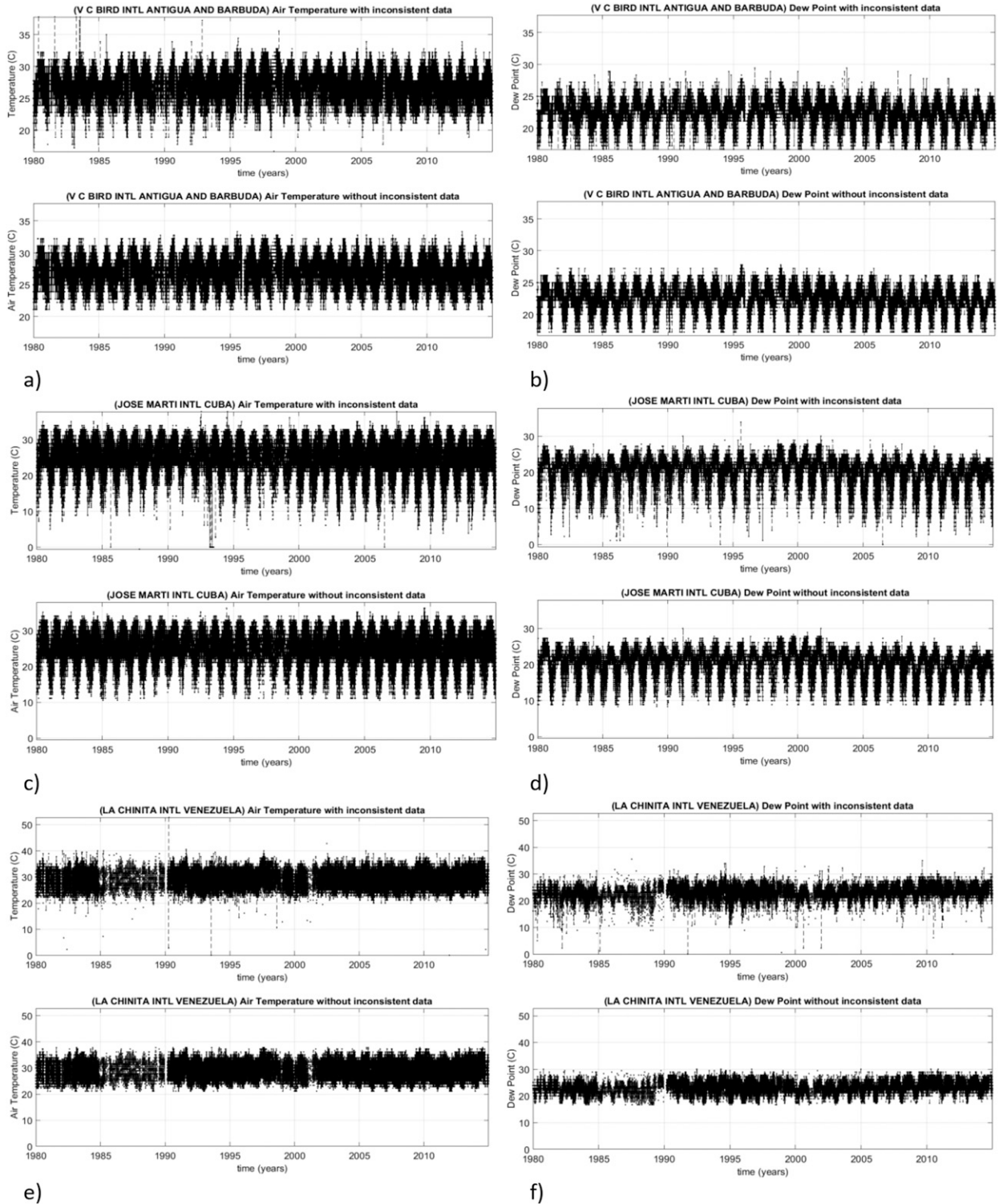
FIG. 2. Original and filtered (left) air temperature and (right) dewpoint for (a),(b) Antigua and Barbuda (example for Lesser Antilles), (c),(d) Cuba (example for Greater Antilles), and (e),(f) Venezuela (example for Mesoamerica).
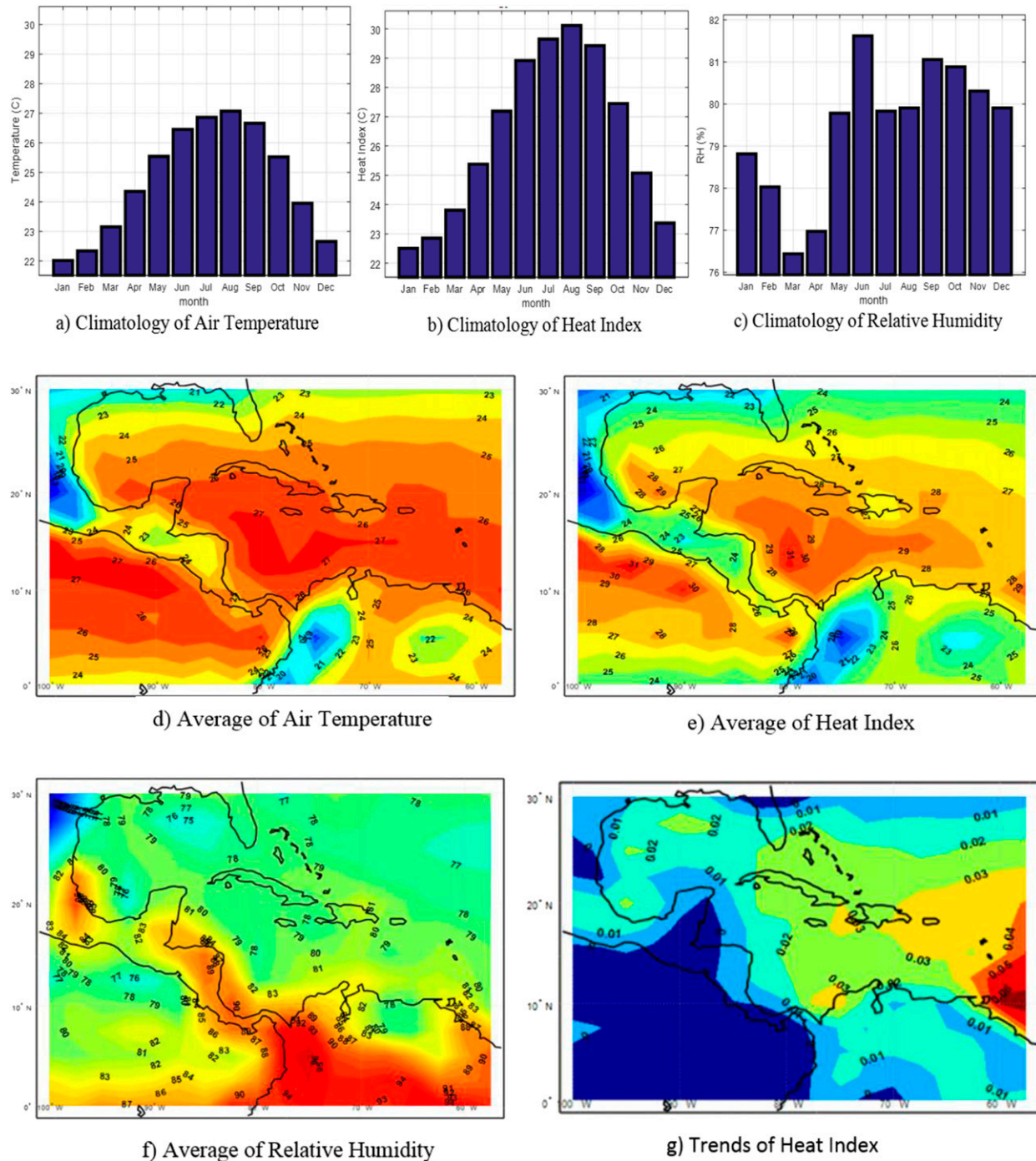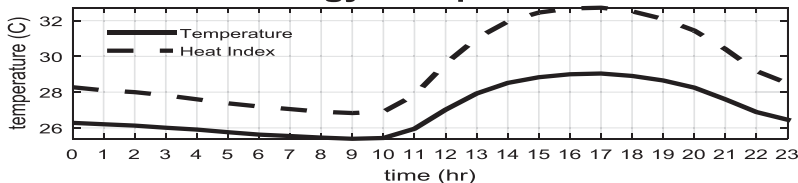
a) Climatology of Air Temperature

b) Climatology of Heat Index

c) Climatology of Relative Humidity

d) Average of Air Temperature

e) Average of Heat Index

f) Average of Relative Humidity

g) Trends of Heat Index

FIG. 3. Climatology of (a) air temperature, (b) heat index, and (c) RH. The average (d) air temperature, (e) heat index, and (f) RH. (g) The trends in the spatial distribution of the heat index. Climatology, grid averages, and grid trends were computed using 6-h NCEP–NCAR data during a 35-yr period (1980–2014).

time when T_{max} occurred. This time interval was selected because H_i is most likely to occur during daytime hours. The 24-h climatology was calculated by computing the average for every hour during the 35-yr dataset. The 24-h climatology indicates that maximum H_i corresponds to T_{max} and approximately the minimum of the RH, whereas the minimum H_i corresponds to the minimum air temperature and
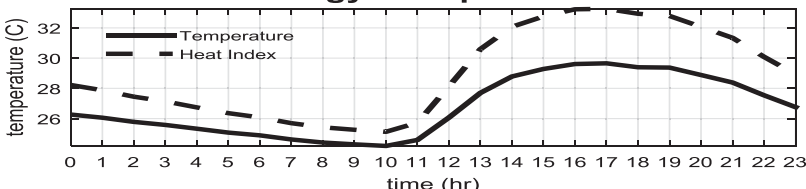
24 hour - Climatology: Temperature and Heat Index
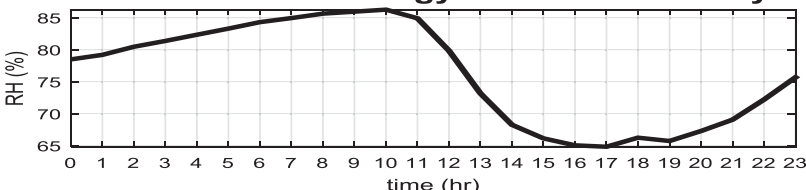

24 hour - Climatology: Relative Humidity
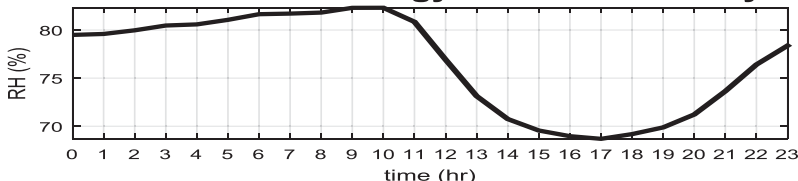
(a) Antigua & Barbuda Station

24 hour - Climatology: Temperature and Heat Index
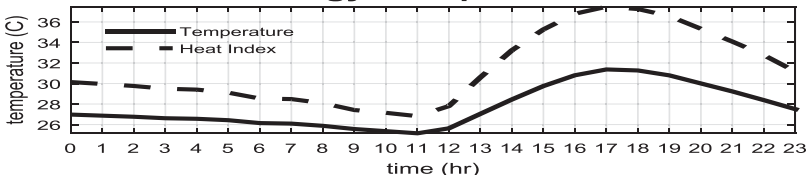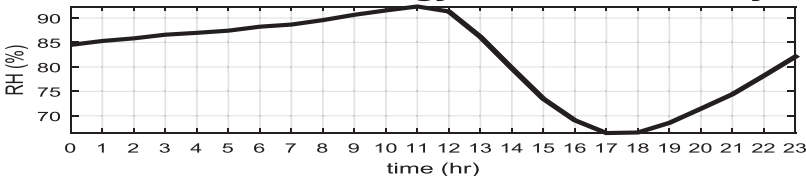

24 hour - Climatology: Relative Humidity

(b) Puerto Rico Station

24 hour - Climatology: Temperature and Heat Index

24 hour - Climatology: Relative Humidity

(c) Colombia Station

FIG. 4. The 24-h climatology of air temperature, heat index, and relative humidity for stations located in (a) Antigua and Barbuda, (b) Puerto Rico, and (c) Colombia. The time is given in UTC, and these figures show the averages of hourly 35-yr data.

about the maximum RH, as shown in Fig. 4. Figure 4 exhibits the 24-h average heat index behavior at three stations: Antigua–Barbuda (top; 17.137°N, 61.793°W), Puerto Rico (middle; 18.417°N, 66°W), and Colombia (bottom; 10.89°N, 74.781°W). These stations correspond to samplings from the Lesser and Greater Antilles, and the Mesoamerica zone, respectively.

d. Trends and climatology of the maximum daytime heat index

The climatology patterns and characteristics of each station were organized into homogenous climate zones to best represent the H_i seasonal variability over different geographical zones and to conduct proper analyses. Self-organizing feature maps (SOFMs) were used to identify the homogeneous climatological patterns. An SOFM is an artificial neural network that uses an unsupervised competitive learning algorithm to organize a set of data into homogenous classes (Hagan et al. 2014; Yip and Yau 2012; Ultsch and Roske 2002). The SOFM suggests that the data can be organized into three homogenous groups that correspond to the different geographical zones. The homogeneous groups were located in the Lesser Antilles, the Greater Antilles, and the Mesoamerica coastal zone. Figure 1 indicates the weather station locations, with the majority of stations located in the coastal areas. The dotted red line in Fig. 1 shows the identified homogenous zones. The SOFM included Miami, Florida (station 12), and Honduras (station 10) within the Greater Antilles zone since their climatological characteristics resemble inherent properties associated with this zone.

The annual time series of a given climate variable usually exhibit an increasing or decreasing trend that is typically represented by a linear function. The slope of the linear function is estimated by parametric or nonparametric methods. The usual parametric method is the least squares method and one of the nonparametric techniques is the Theil–Sen method (Zaman et al. 2015). The nonparametric method is robust to the presence of outliers and both methods are affected by the autocorrelation of the underling time series. Hence, the slope significance is sensitive to the presence of the autocorrelation of the climate data. It is known that when the autocorrelation of the time series is high, the t statistic associated with the slope is overestimated and consequently the significance of the slope is also overestimated. To avoid this problem, the autocorrelation of the data should be parameterized and included in the regression model (Abraham and Ledolter 2006).

Assuming the studied climate time series have moderate autocorrelation, a linear regression methodology was applied for computing trends, and the daily averages were used to calculate the climatology for H_i. A straight line was fitted to H_i to measure the trend. The slope of the straight line was tested to determine whether or not it is statistically significant. Daily heat indices were also aggregated to compute monthly and annual time series to estimate trends. Data were also aggregated for homogenous zones to estimate trends for the Lesser and Greater Antilles and also for the Mesoamerica zone.

e. Analysis of heat index extreme events

In the MAC region, it is common to find places with extreme hot behavior during the daytime. However, the critical weather conditions occur when the hot conditions are also maintained during the nighttime. Therefore, *the HIEE in the MAC region is defined as an extraordinary hot event where the maximum-daytime heat index and the minimum-nighttime heat index both exceed the corresponding 97th percentiles and this hot event must persist for at least two consecutive days*. The 97th percentiles should be derived with the analysis of at least 30 yr of hourly data, and this percentile was determined after computing all the potential extreme heat events based on a q percentile, where q varies from 95 to 99 in increments of 1. An HIEE must be a rare event and according to the NWS (Robinson 2001) is such that a station should have less than three extreme heat events per decade. Thus, an approximation of a rare event definition for the MAC region would be a station that has 10 or fewer HIEEs during 3.5 decades, and the corresponding percentile that meets this criterion was the 97th. Values about the 97th percentile were not selected because some important hot–humid events may be missing. Thus, when a high percentile is applied, it is difficult for the event to maintain the hot and humid levels for 2 days to qualify as an extreme event. On the other hand, values below the 97th percentile were also not selected because they do not correspond to the rare-event criterion.

4. Results

Results for analyzing the H_i in the MAC region were organized into three parts. The first part describes the climate characteristics of the stations and also the characteristics for each homogenous region. The second part presents results of trend analysis and climatology patterns of H_i, and the third part presents the analysis of heat index extreme events.

a. Station climate characteristics

Table 1 summarizes the climate characteristics for each of the studied stations. In each country, the station that provides the most complete dataset was selected and the largest sample size was found at the Miami International Airport (12 695 days) and the smallest was in Guadeloupe (9068 days). The station that exhibits the largest T_{max} average was La Chinita International Airport in Maracaibo, Venezuela (32.8°C, 91°F), whereas

TABLE 2. The climate characteristics of the MAC zones.

Zone	Avg filtered data (No. of days)	Avg air temperature T_{max} (°C)	Avg RH (%)	Avg H_i (°C)	Avg diff $(H_i - T_{max})$ (°C)
Lesser Antilles	87% (11 160)	29.4	68.1	33.5	4.1
Greater Antilles	94% (12 026)	29.9	61.3	33.3	3.4
Mesoamerican coastal zone	93.7% (11 984)	31.7	61.7	37.1	5.4

the station with the lowest air temperature average was Miami International Airport (28.6°C, 83.4°F). This result was expected since these stations are located at about sea level and Miami is at the highest latitude (25.8°N) and La Chinita at the lowest latitude (10.6°N). Pointe-à-Pitre Le Raizet Airport in Guadalupe shows the highest average RH of 69.8%, and Toussaint Louverture International Airport in Port-au-Prince, Haiti, exhibited the lowest average RH (51.4%). La Chinita International Airport shows the largest average H_i [38.3°C (100.9°F)]; whereas Miami International Airport shows the smallest average of H_i [31°C (87.8°F)]. This result was expected because temperature has a greater influence than RH on H_i. The difference between H_i and T_{max} was computed. The largest difference [6.2°C (11.2°F)] was reported at Ernesto Cortissoz International Airport in Soledad, Colombia. The average temperature at La Chinita is larger than that at Ernesto Cortissoz, and it was expected that the largest difference should be found at La Chinita. However, the RH humidity is larger at Ernesto Cortissoz and it caused the largest difference at Ernesto Cortissoz. On the other hand, the smallest difference [2.4°C (4.3°F)] was found at Miami International Airport, since the temperature was the dominant parameter in the estimation of the heat index.

Table 2 shows a summary of the characteristics of each of the Mesoamerican and Caribbean zones, and includes the averages of sample size, T_{max}, RH, H_i average, and average of the difference between H_i and T_{max}. The Lesser and Greater Antilles exhibited similar characteristics, with the exception of RH, as the Lesser Antilles showed on average the largest RH since they are very small islands with intense rainfall and ocean evaporation dominates in this zone. In terms of T_{max}, the averages for the Lesser and Greater Antilles were almost the same, having the smallest average maximum air temperature [29.4°C (84.9°F)] in the studied area, while the Mesoamerica zone exhibits the largest average of T_{max} [31.7°C (89°F)]. The Greater Antilles exhibit the smallest difference $(H_i - T_{max})$, about 3.4°C (6.1°F). On the other hand, the Mesoamerica zone showed the largest averages of H_i, T_{max}, [37.1°C (98.8°F), 31.7°C (89°F)] and the largest difference [5.4°C (9.8°F)]. Thus, it is likely that people

living in Mesoamerican countries are exposed to a higher risk than those living in Caribbean countries (OSHA 2016).

b. Trends and climatology

The T_{max} time series are shown in Fig. 5a, while Fig. 5b shows H_i for the MAC region based on station data. A linear trend was computed for each of the time series and significant trends were observed: T_{max} and H_i of 0.02°C yr^{-1} (0.04°F yr^{-1}) and 0.05°C yr^{-1} (0.10°F yr^{-1}), respectively. Trenberth et al. (2007) and Jury (2015) reported a similar temperature trend for the Caribbean and Puerto Rico, respectively. The trend and climatology for the RH are given in Figs. 5c and 5d, respectively. Figure 5c shows that RH has some fluctuation around the mean with no significant trend. Figure 5d shows that the climatology of the RH follows a bimodal distribution and starts ascending in March until reaching its first peak in June with a small reduction in July. The largest peak occurs in November and then starts descending until completing the cycle in March. Angeles et al. (2010) show that the Caribbean rainfall climatology exhibits a small reduction in July and they claim that the rainfall bimodal behavior is influenced by the vertical wind shear and the aerosol particles. Thus, it is likely that the RH bimodal pattern is also influenced by the abovementioned variables. Figure 5e exhibits the climatology of T_{max} and this pattern is similar to the H_i climatology. Figure 5f shows the climatology of H_i for the entire region, and follows a unimodal distribution. The H_i reduction observed in July is caused by the reduction in RH and the largest peak in H_i is also caused by the increase in RH; however, the largest value in H_i occurred earlier than the peak in RH, because the air temperature is the dominant variable and starts decreasing in September. Figure 5g shows the difference between H_i and T_{max} for the entire region and exhibits a similar pattern to H_i. The difference between H_i and T_{max} varies between 2°C (3.6°F) in January and 6°C (10.8°F) in August. These analyses show how the potential periods for extreme hot events are more likely to take place during the rainy season and less likely to occur during the dry season. This observation is in agreement with reports presented in other parts of the world (Dixon 1998; Rakib 2013).

a) Monthly Maximum Air Temperature

b) Monthly Maximum Heat Index

c) Monthly Minimum Relative Humidity

d) Climatology of Relative Humidity

e) Climatology of Air Temperature

f) Climatology of Heat Index

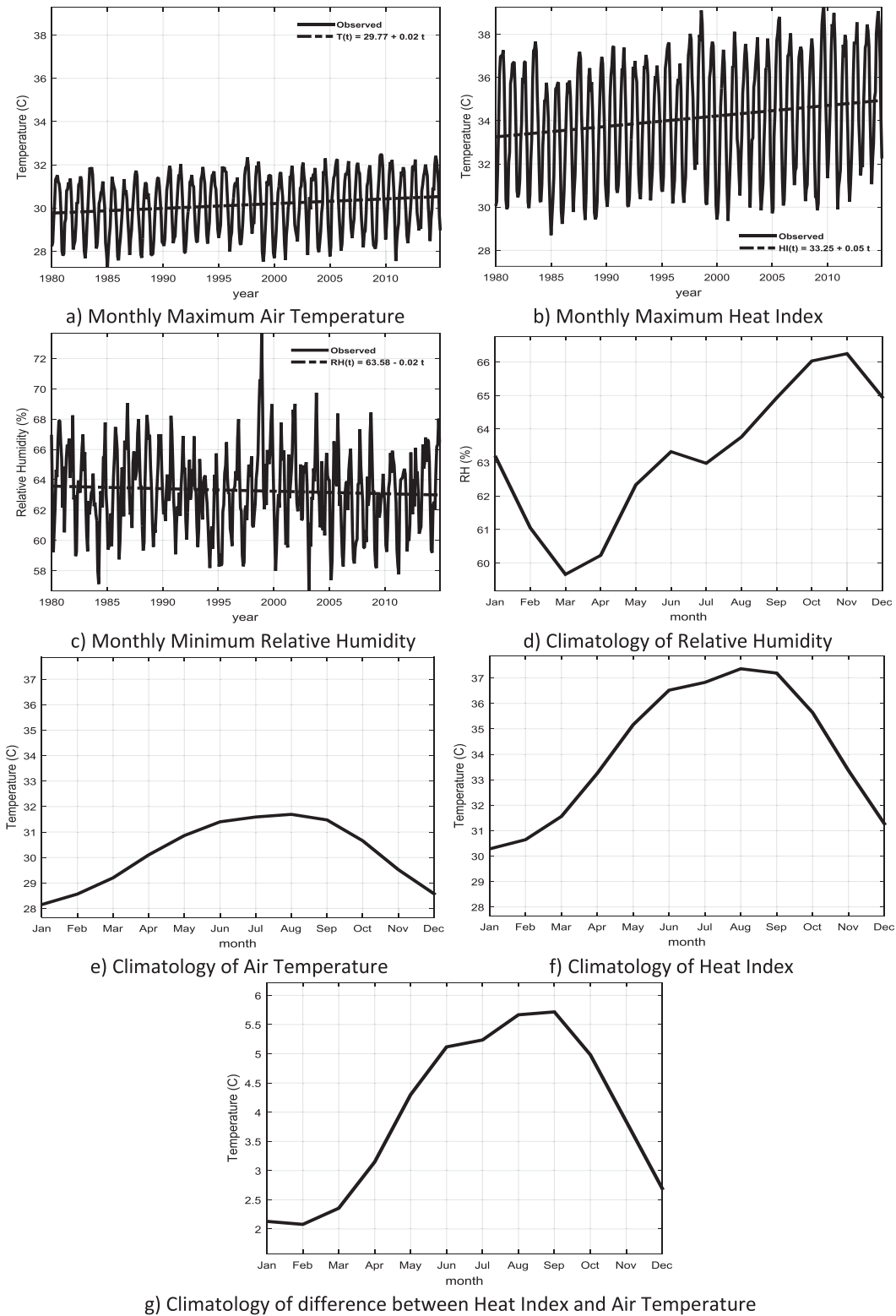g) Climatology of difference between Heat Index and Air Temperature

FIG. 5. Trends in monthly (a) maximum air temperature, (b) maximum heat index, and (c) minimum RH. The climatology of (d) RH, (e) maximum air temperature, and (f) maximum heat index. (g) The difference of two climatological variables: the maximum heat index and maximum air temperature. The RH presented is the one that corresponds to the hourly maximum air temperature.
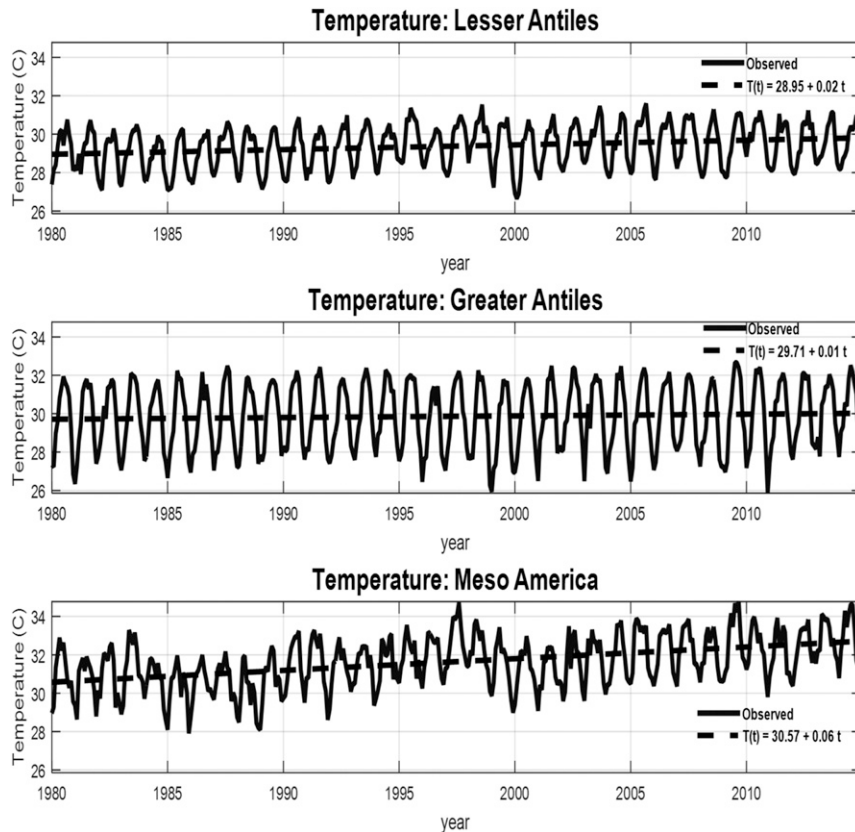
FIG. 6. Trends of the maximum air temperature for (top) the Lesser Antilles, (middle) the Greater Antilles, and (bottom) Mesoamerica.

Figures 6 and 7 show the T_{max} and H_i trends for the three MAC zones, respectively. The trends for T_{max} and H_i in each zone are given in Table 3, which indicates that in the Lesser Antilles the trends of T_{max} and H_i are significant and show increasing trends of $0.02°C\,yr^{-1}$ ($0.03°F\,yr^{-1}$) and $0.04°C\,yr^{-1}$ ($0.08°F\,yr^{-1}$), respectively. In addition, the trends for both T_{max} and H_i in Mesoamerica are significant, with a large rate of $0.06°C\,yr^{-1}$ ($0.11°F\,yr^{-1}$) and $0.16°C\,yr^{-1}$ ($0.29°F\,yr^{-1}$), respectively. However, the trends for the maximum temperature and heat index in the Greater Antilles are not significant, as shown in Table 3. In addition, Fig. 8 and Table 3 show that RH has no significant trend, with the exception of the Lesser Antilles, exhibiting a reduction of $0.09\%\,yr^{-1}$.

Climatologies of T_{max}, RH, and H_i are shown in Fig. 9. It is noted that climatologies for both T_{max} and H_i follow a bimodal distribution for Mesoamerica; however, a unimodal distribution is shown for the Caribbean Islands (Lesser and Greater Antilles). On the other hand, the climatology for the Lesser Antilles shows the largest RH with the smallest H_i, since its T_{max} values are about the smallest over the entire region of study. The climatology of the RH follows a bimodal distribution and starts ascending in March until obtaining its first peak in June or in July, followed by a small reduction, and then continues rising until achieving its maximum peak in October or in November (Fig. 9, bottom). It can be observed that the Mesoamerica region is the hottest zone, followed by the Greater Antilles and then the Lesser Antilles. On the other hand, the Lesser Antilles revealed the largest RH, followed by Mesoamerica, and the smallest RH (during summer) is in the Greater Antilles.

c. Analysis of heat index extreme events

Table 4 shows the number of extreme hot events for each station when the percentile varies from the 95th to the 99th. Thus, the 97th percentile is the one that meets the rare-event criterion and detects extreme events. This percentile provides 45 extreme events for the region, and it is enough data to perform an analysis of the extreme events.

Observations collected during 1000–2200 UTC were associated with daytime events, whereas observations that fall outside this range were used to identify nighttime hot events. Based on 35 yr of hourly
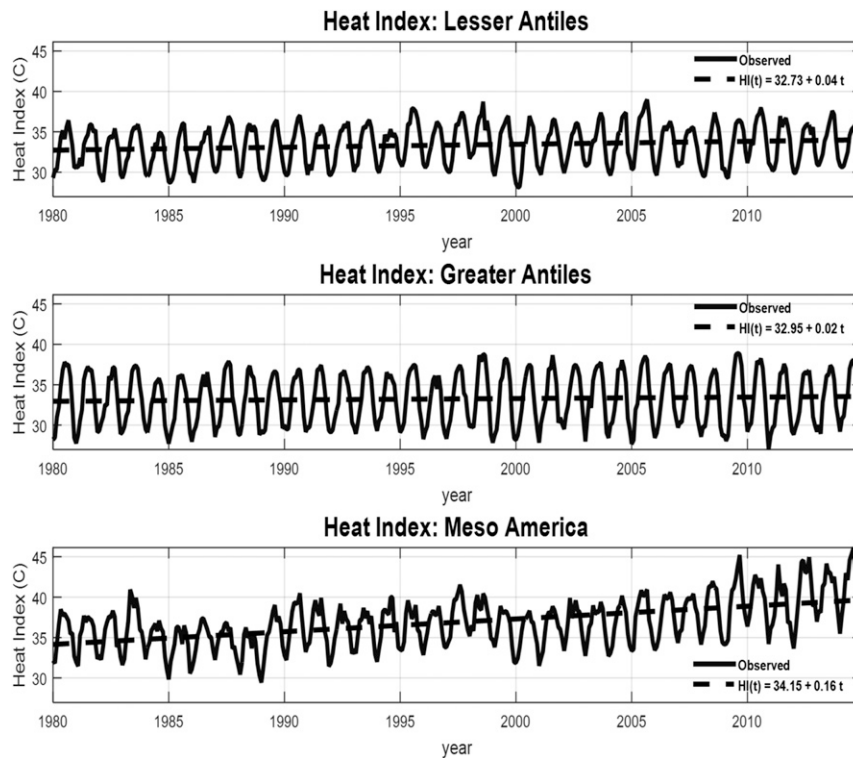
FIG. 7. As in Fig. 6, but for the maximum heat index.

data, the maximum and the minimum thresholds for each station were computed, and they are shown in Table 5. The threshold for each station varies since each station exhibits different local climatological conditions. On average Mesoamerican countries exhibit the hottest events [>46.0°C (114.8°F)] during the daytime. The Lesser Antilles exhibits the hottest nighttime events [>30.7°C (87.3°F)]. The difference between the average daytime and nighttime thresholds is greatest [17.5°C (31.5°F)] in Mesoamerica and smallest [8.1°C (14.6°F)] in the Lesser Antilles. A practical contribution of this work is to suggest thresholds for identifying the occurrence of HIEE in the MAC region.

The major characteristics of the HIEE are the duration d and the intensity, which are the parameters that determine the severity of the hot events. For a given station, the relative intensity (ri) was used to perform analysis (instead of absolute intensity) since the intensity depends on the local climate characteristics. The relative intensity is the number of degrees by which the maximum heat index exceeds the threshold (or 97th percentile) of a given station, whereas the absolute intensity is the actual intensity observed at a station. The relative intensity was used to be able to compare the strength of HIEE that occurs for different climate conditions. Thus, to characterize the severity of an extreme hot event, it is required to jointly study the duration and intensity of the event, and the joint probability distribution is given in Table 6 and Fig. 10.

The correlation between duration and relative intensity is 0.19, indicating that there is a weak linear dependency between these variables. Although the correlation is weak, the analysis of HIEE should be performed using simultaneous duration and relative intensity, since a nonlinear dependency may exist between these variables. The joint probability distribution can be used to answer practical questions related to the duration and intensity of a given HIEE. For instance, what would be the possibility that an extreme event will last 3 days or less with a relative intensity equal or less than 3°C (5.4°F)? The joint probability distribution indicates that 71% of the extreme events in the MAC region meet these conditions.

The joint probability distribution suggests that a severe HIEE occurs when the relative intensity is greater than 3°C (5.4°F) and persists for more than 4 days, and the probability of this event to occur is 0.022. Only one event out of 45 extreme events occurred during the 35-yr study period, in September 2009 in Antigua and Barbuda and this event lasted 4.5 days and had a 4°C (7.2°F) relative intensity. On the

TABLE 3. Trends and *p* values for the Lesser and Greater Antilles and Mesoamerica zones.

Zone	Max air temperature		Max daytime H_i		RH	
	Slope (°C yr⁻¹)	*p* value	Slope (°C yr⁻¹)	*p* value	Slope (% yr⁻¹)	*p* value
Lesser Antilles	0.02	0.00	0.04	0.00	−0.09	0.00
Greater Antilles	0.01	0.29	0.02	0.27	0.02	0.22
Mesoamerica	0.06	0.00	0.16	0.00	−0.00	0.92

other hand, the most likely HIEE is that which shows a relative intensity of less than 3°C (5.4°F) with a duration of less than 3 days, and the probability of this event occurring is 0.55.

The last column in Table 6 shows the marginal duration probability distribution of HIEE, whereas the last row exhibits the marginal probability distribution of the relative intensity. It was found that the average duration of a heat index extreme event was 2.43 days with a standard deviation of 0.57 days. The mean of the relative intensity was 2.44°C (4.39°F) and the standard deviation was 1.22°C

(2.20°F). The duration probability distribution indicates that 82% of heat events last fewer than 3 days, and the relative intensity distribution shows that 80% of heat events exhibit a relative intensity less than 4°C (7.2°F).

The third important characteristic of the HIEE is the annual and monthly frequencies. Figure 11a shows that the annual frequency of extreme events has intensified since 1991, with the highest incidences recorded in 1995, 1998, 2005 and 2010, and these years coincide with the occurrence of ENSO, especially during its cool phase (Null 2017). Figure 11b indicates that the HIEEs have
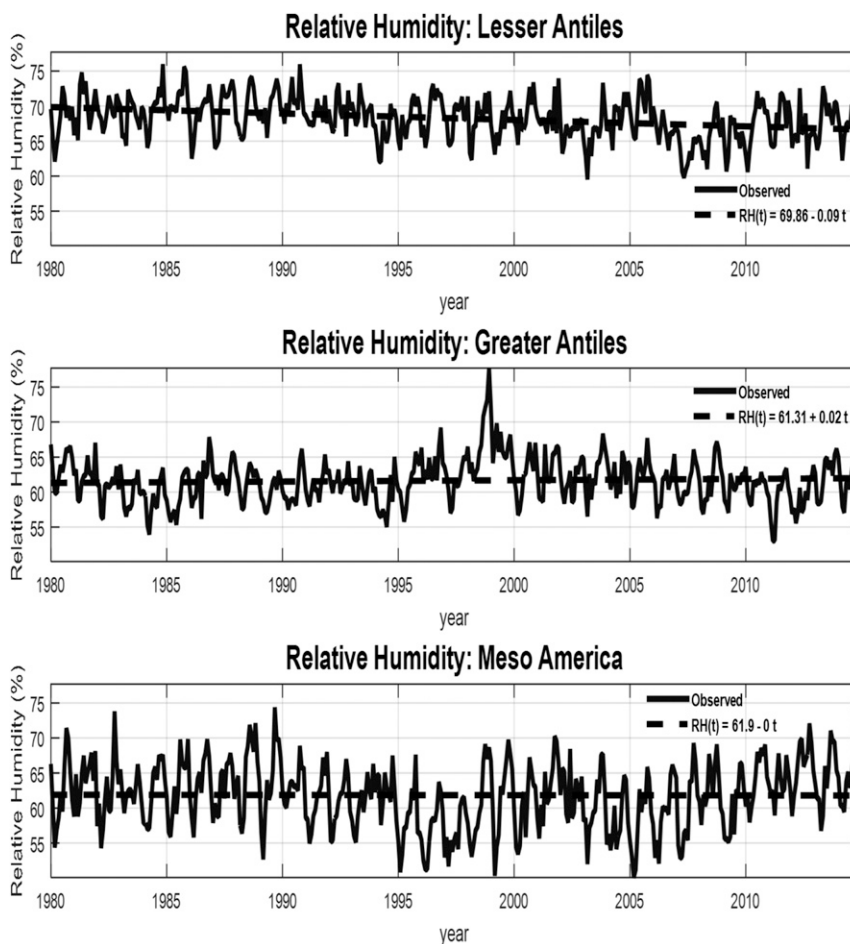

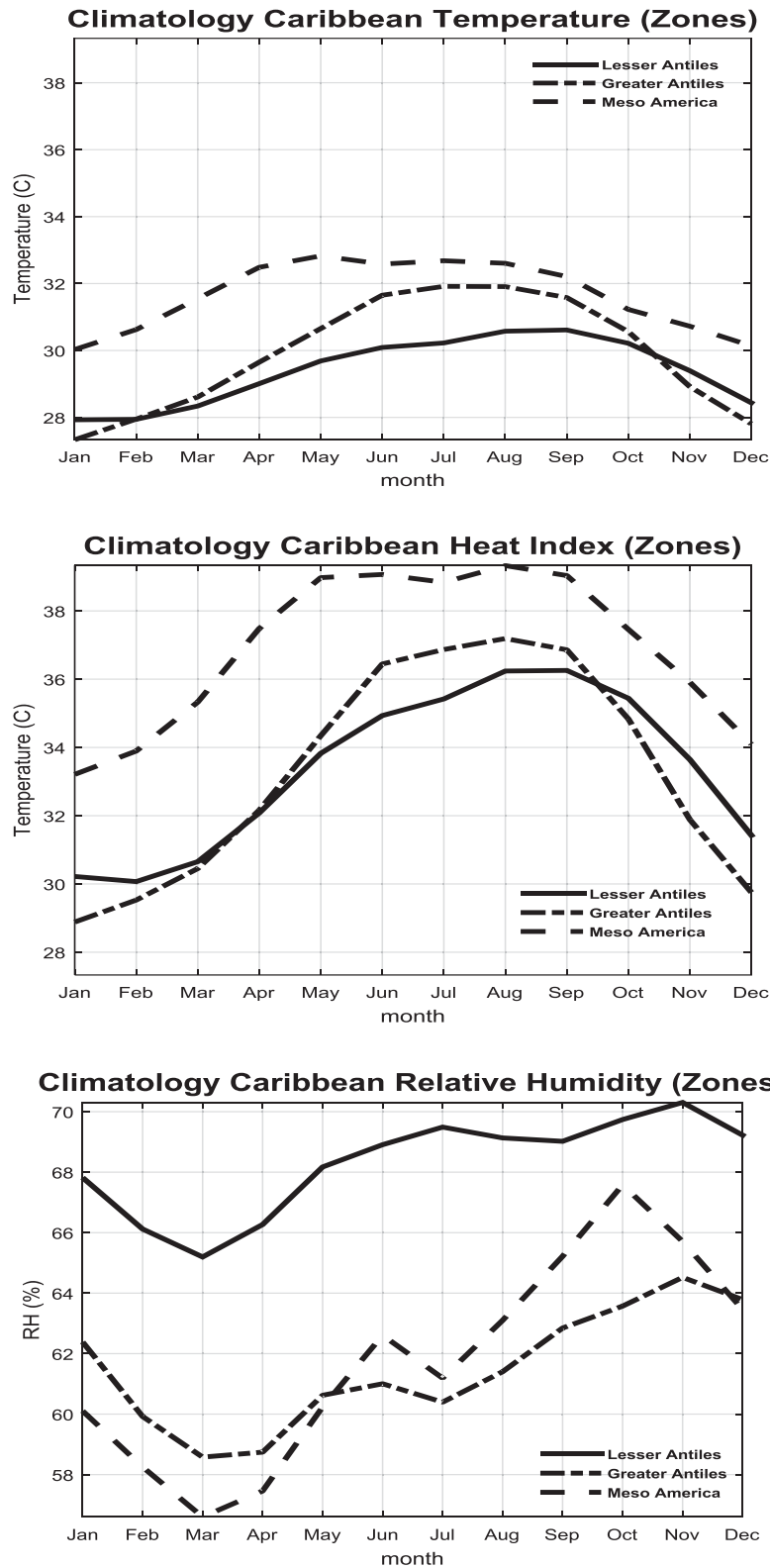FIG. 8. As in Fig. 6, but for the RH associated with the maximum air temperature.

FIG. 9. Monthly climatology based on (top) daily maximum air temperature, (middle) daily maximum heat index, and (bottom) daily RH associated with the maximum air temperature.

TABLE 4. Heat index extreme events per station and per percentile.

Station and location	HI extreme events 95th percentile	HI extreme events 96th percentile	HI extreme events 97th percentile	HI extreme events 98th percentiles	HI extreme events 99th percentile
Robert L. Bradshaw International Airport, Basseville, St. Kitts and Nevis	12	4	3	2	1
V. C. Bird International Airport, St. John's, Antigua and Barbuda	14	12	10	4	3
Pointe-à-Pitre Le Raizet Airport, Pointe-à-Pitre, Guadeloupe	4	2	0	0	0
Martinique Aimé Césaire International Airport, Le Lamentin, Martinique	2	2	1	1	0
E. T. Joshua Airport, Kingstown, St. Vincent	10	9	1	0	0
Luis Muñoz Marín International Airport, San Juan, Puerto Rico	11	8	4	3	0
Cibao International Airport, Santiago de los Caballeros, Dominican Republic	6	4	1	0	0
Sangster International Airport, Montego Bay, Jamaica	18	10	5	0	0
Toussaint Louverture International Airport, Port-au-Prince, Haiti	10	6	2	2	0
Golosón International Airport, La Ceiba, Honduras	9	7	2	1	1
Jose Marti International Airport, Havana, Cuba	2	1	1	1	0
Miami International Airport, Miami	17	9	6	3	1
La Chinita International Airport, Maracaibo, Venezuela	14	9	6	4	3
Ernesto Cortissoz International Airport, Soledad, Colombia	5	3	3	1	1
Valladolid Airport, Villanubla, Mexico	10	0	0	0	0
Total No. of HI extreme events	144	86	45	22	10

occurred during the rainy season with the largest frequency occurring in August. During the rainy season in the years 1982 and 1987, El Niño events were very strong and moderate, respectively; but their effects were not reflected in the frequency of the HIEEs. Hence, the frequency of HIEE in the MAC is partially modulated by ENSO. Additional research is needed to identify the remaining factors that contribute to the development of HIEE.

5. Summary and conclusions

Ground station data were used to estimate the heat index over the Caribbean and Mesoamerican region for a period of 35 yr. A daily value of H_i was computed based on hourly observations of air temperature and RH.

The H_i trend shows a notable increase during the studied period. The trend of the heat index is more prominent in Mesoamerica than in the Caribbean countries.

Values of H_i were higher in Mesoamerica, followed by the Greater Antilles and then by the Lesser Antilles. Climatology of H_i follows a unimodal distribution for the entire Caribbean Islands with the largest values occurring in August. Mesoamerican countries exhibited a bimodal H_i distribution with the first peak in May and the second in August. The climatology of the RH in the MAC region follows a bimodal distribution with the largest peak in June and the second peak occurring during the months of October–November with the smallest RH occurring in March. In the MAC region the RH exhibits fluctuations about the mean with no significant trend. The climatology

TABLE 5. Heat index thresholds (the values in the last three columns are the averages of all of the stations in their respective groups: e.g., Venezuela, Columbia, and Mexico are one group).

Station and location	Thresholds (97th percentile) Min (°C)	Thresholds (97th percentile) Max (°C)	Avg min (°C)	Avg max(°C)	Avg diff in thresholds (°C)
Robert L. Bradshaw International Airport, Basseville, St. Kitts and Nevis	31.1	38.7	30.7	38.8	8.1
V. C. Bird International Airport, St. John's, Antigua and Barbuda	31.5	38.2			
Pointe-à-Pitre Le Raizet Airport, Pointe-à-Pitre, Guadeloupe	29	38.8			
Martinique Aimé Césaire International Airport, Le Lamentin, Martinique	30.2	39.1			
E. T. Joshua Airport, Kingstown, St. Vincent	31.7	39			
Luis Muñoz Marín International Airport, San Juan, Puerto Rico	30.1	39.5	27.7	40.2	12.5
Cibao International Airport, Santiago de los Caballeros, Dominican Republic	23.9	39.6			
Sangster International Airport, Montego Bay, Jamaica	30.9	42.3			
Toussaint Louverture International Airport, Port-au-Prince, Haiti	28.7	40.3			
Golosón International Airport, La Ceiba, Honduras	24.6	41.1			
Jose Marti International Airport, Havana, Cuba	24.5	40			
Miami International Airport, Miami	31.2	38.7			
La Chinita International Airport, Maracaibo, Venezuela	31.9	45.2	28.5	46.0	17.5
Ernesto Cortissoz International Airport, Soledad, Colombia	31.9	43.2			
Valladolid Airport, Villanubla, Mexico	21.7	49.7			

of H_i ranges from 30°C (86°F) to 37°C (98.6°F), the RH varies from 60% to 67%, and the T_{max} range from 28°C (82.4°F) to 32°C (89.6°F).

The HIEE in the MAC region is defined as an extraordinary hot event where the maximum-daytime heat index and the minimum-nighttime heat index both exceed the corresponding 97th percentiles and this hot event must persist for at least two consecutive days. The average thresholds for the minimum and the maximum heat indices for the Lesser Antilles are 30.7° and 38.8°C (87.3° and 101.8°F), respectively; for the Greater Antilles they are 27.7° and 40.2°C (81.9° and 108.0°F); and for Mesoamerica they are 28.5° and 46.0°C (83.3° and 114.8°F). On average, Mesoamerican countries exhibit the hottest daytime events [>46.0°C (114.8°F)] and the Lesser Antilles exhibit the hottest nighttime events [>30.7°C (87.3°F)]. On average, the difference between the daytime and nighttime thresholds is greatest in Mesoamerica [17.5°C (31.5°F)] and smallest in the Lesser Antilles [8.1°C (14.6°F)].

The duration and relative intensity of HIEEs were used to characterize these events. The severity of an HIEE

cannot be determined just by looking at the duration of the relative intensity alone. It is necessary to observe the strength of both variables simultaneously; that is, it is recommended that the joint probability distribution be used to estimate the likelihood that a HIEE develops at a certain level of strength.

The correlation between the duration and relative intensity is 0.19, indicating that there is a weak linear dependency between these variables. Although the

TABLE 6. Bivariate and marginal probability distributions of the HIEE.

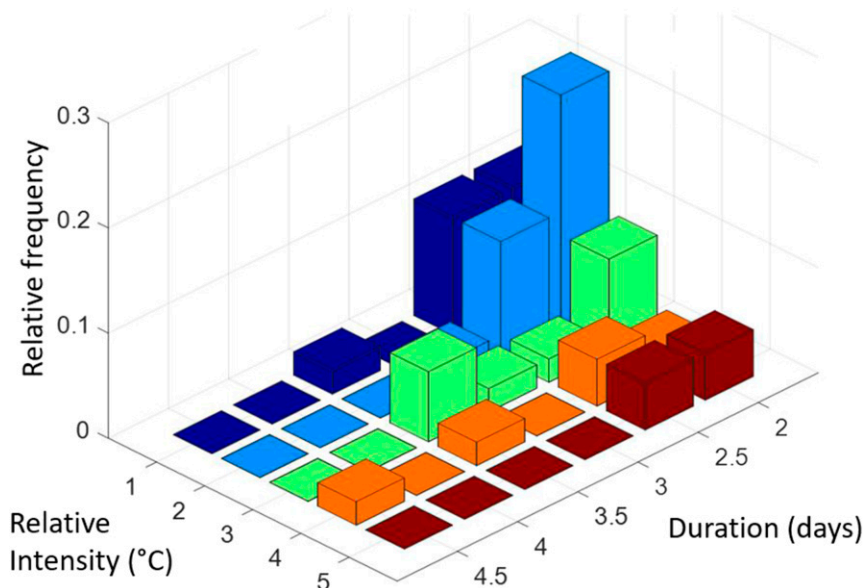| $f_{D,ri}(d, ri)$		ri (°C) 1	2	3	4	5	$f_D(d)$
d (days)	2.0	0.1111	0.2222	0.0889	0.0222	0.0444	0.4889
	2.5	0.1111	0.1111	0.0222	0.0444	0.0444	0.3333
	3.0	0	0.0222	0.0222	0	0	0.0444
	3.5	0.0222	0	0.0667	0.0222	0	0.1111
	4.0	0	0	0	0	0	0
	4.5	0	0	0	0.0222	0	0.0222
$f_{ri}(ri)$		0.2444	0.3556	0.2	0.1111	0.0889	

FIG. 10. Bivariate probability distribution of duration (days) and relative intensity of heat index (°C) extreme events.

correlation is weak, the analysis of HIEE should be performed using duration and relative intensity simultaneously, since a nonlinear dependency may exist between these variables. The joint probability distribution suggests that a severe HIEE occurs when the relative intensity is greater than 3°C (5.4°F) and persists for more than 4 days, and the probability of this event occurring is 0.022. Only 1 event out of 45 extreme events occurred during the 35-yr study period, in September 2009 in Antigua and Barbuda, and it lasted 4.5 days and had a 4°C (7.2°F) relative intensity. On the other hand, the most likely HIEE is the one that shows a

relative intensity of less than 3°C (5.4°F) with a duration of fewer than 3 days, and the probability of this event occurring is 0.55.

The annual frequency of HIEE has intensified since 1991 and the years with high incidences coincide with the cool phase of ENSO. However, there were a few years when ENSO episodes occurred and their effects were not reflected in the frequency of the HIEEs. Consequently, additional research is needed to better understand the climate parameters that control the annual frequency of HIEE.

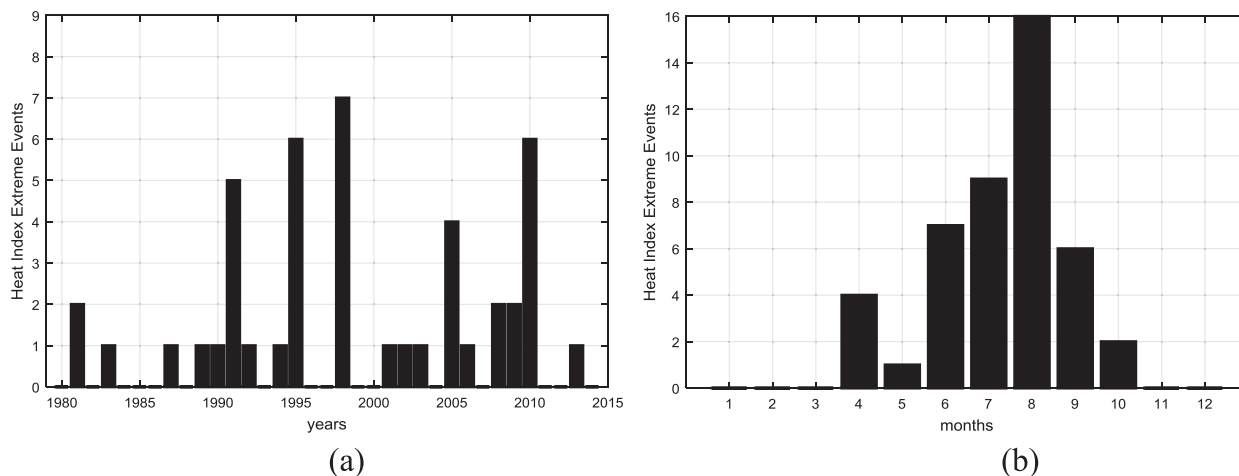It should be noted that this study is limited in the sense that no validation was perform with health-related data,

FIG. 11. The (a) annual and (b) monthly frequencies of heat index extreme events.

and no comparison was conducted with other thermal stresses.

REFERENCES

Abraham, B., and J. Ledolter, 2006: *Introduction to Regression Modeling.* Thomson Brooks/Cole, 433 pp.

Alexandersson, H., 1986: A homogeneity test applied to precipitation data. *J. Climatol.*, **6**, 661–675, doi:10.1002/joc.3370060607.

American Meteorological Society, 2015: Heat wave. Glossary of Meteorology, http://glossary.ametsoc.org/wiki/Heat_wave.

Anderson, G. B., M. L. Bell, and R. D. Peng, 2013: Methods to calculate the heat index as an exposure metric in environmental health research. *Environ. Health Perspect.*, **121**, 1111–1119, doi:10.1289/ehp.1206273.

Angeles, M. E., J. E. González, N. D. Ramírez-Beltrán, C. A. Tepley, and D. E. Comarazamy, 2010: Origins of the Caribbean rainfall bimodal behavior. *J. Geophys. Res.*, **115**, D11106, doi:10.1029/2009JD012990.

Dixon, R. W., 1998: A heat index climatology for the southern United States. *Natl. Wea. Dig.*, **22** (1), 16–21, http://nwafiles.nwas.org/digest/papers/1997/Vol22No1/Pg16-Dixon.pdf.

Fanger, P. O., 1970: *Thermal Comfort.* Danish Technical Press, 244 pp.

Gallagher, C., R. Lund, and M. Robbins, 2013: Changepoint detection in climate time series with long-term trends. *J. Climate*, **26**, 4994–5006, doi:10.1175/JCLI-D-12-00704.1.

Giannini, A., Y. Kushnir, and M. A. Cane, 2001: Seasonality in the impact of ENSO and the North Atlantic high on Caribbean rainfall. *Phys. Chem. Earth*, **26B**, 143–147, doi:10.1016/S1464-1909(00)00231-8.

Goldenberg, S. B., C. W. Landsea, A. M. Mestas-Nuñez, and W. M. Gray, 2001: The recent increase in Atlantic hurricane activity: Causes and implications. *Science*, **293**, 474–479, doi:10.1126/science.1060040.

González-Cruz, J., P. Sequera, Y. Molina, R. Picon, J. Pillich, A. T. Ghebreegziabhe, and B. Bornstein, 2013: Climate and energy vulnerability in coastal regions: The case for U.S. Pacific and Northeast Corridor coastal regions. *Climate Vulnerability: Understanding and Addressing Threats to Essential Resources*, R. A. Pielke, Sr., Ed., Academic Press, 3–35.

Hagan, M. T., H. B. Demuth, M. Beal, and O. De Jesus, 2014: *Neural Network Design.* 2nd ed. PWS Publishing, 800 pp.

Jury, M. R., 2015: Climatic trends in Puerto Rico: Observed and projected since 1980. *Climate Res.*, **66**, 113–123, doi:10.3354/cr01338.

Loughnan, M., N. Tapper, and T. Phan, 2014: Identifying vulnerable populations in subtropical Brisbane, Australia: A guide for heatwave preparedness and health promotion. *ISRN Epidemiol.*, 2014, 821759, doi:10.1155/2014/821759.

Méndez-Lázaro, P., O. Martínez-Sánchez, R. Méndez-Tejeda, E. Rodríguez, E. Morales, and N. Schmitt-Cortijo, 2015: Extreme heat events in San Juan Puerto Rico: Trends and variability of unusual hot weather and its possible effects on ecology and society. *J. Climatol. Wea. Forecasting*, **3**, 135, doi:10.4172/2332-2594.1000135.

Menne, M. J., C. N. Williams Jr., and R. S. Vose, 2009: The U.S. Historical Climatology Network monthly temperature data, version 2. *Bull. Amer. Meteor. Soc.*, **90**, 993–1007, doi:10.1175/2008BAMS2613.1.

Met Office, 2015. Heatwave. Met Office, accessed 1 May 2015, http://www.metoffice.gov.uk/learning/learn-about-the-weather/weather-phenomena/heatwave.

NCEI, 2016: NCEI GIS map portal. National Centers for Environmental Information, accessed 20 February 2016, https://gis.ncdc.noaa.gov/map/viewer/#app=cdo.

NCEP, 2016a: NCEP/NCAR Reanalysis 1: Summary. National Centers for Environmental Prediction, accessed 20 February 2016, http://www.esrl.noaa.gov/psd/data/gridded/data.ncep.reanalysis.html.

——, 2016b: Temporal coverage. NCEP/NCAR Reanalysis 1: Summary. Earth System Research Laboratory, accessed 11 October 2016, http://www.esrl.noaa.gov/psd/data/gridded/data.ncep.reanalysis.html#temp.

Null, J., 2017: El Niño and La Niña years and intensities: Based on oceanic Niño index (ONI). Accessed 14 June 2017, http://ggweather.com/enso/oni.htm.

NWS, 2016: What is the heat index? Accessed 22 January 2016, http://www.weather.gov/ama/heatindex.

——, 2017: Heat watch and warning. Accessed 5 June 2017, http://www.nws.noaa.gov/om/heat/ww.shtml.

OSHA, 2016: Weather. Rest. Shade: OSHA's campaign to keep workers safe in the heat. Accessed 24 July 2016, https://www.osha.gov/SLTC/heatillness/index.html.

Peterson, T. C., and Coauthors, 1998a: Homogeneity adjustments of in situ atmospheric climate data: A review. *Int. J. Climatol.*, **18**, 1493–1517, doi:10.1002/(SICI)1097-0088(19981115)18:13<1493::AID-JOC329>3.0.CO;2-T.

——, R. Vose, R. Schmoyer, and V. Razuvaev, 1998b: Global Historical Climatology Network (GHCN) quality control of monthly temperature data. *Int. J. Climatol.*, **18**, 1169–1179, doi:10.1002/(SICI)1097-0088(199809)18:11<1169::AID-JOC309>3.0.CO;2-U.

Portier, C. J., and Coauthors, 2010: A human health perspective on climate change: A report outlining the research needs on the human health effects of climate change. Environmental Health Perspectives and National Institute of Environmental Health Sciences Rep., 80 pp., https://www.niehs.nih.gov/health/materials/a_human_health_perspective_on_climate_change_full_report_508.pdf.

Rakib, Z. B., 2013: Extreme temperature climatology and evaluation of heat index in Bangladesh during 1981-2010. *J. Pres.Univ.*, **2B** (2), 84–95, http://presidency.edu.bd/uploads/Article012.pdf.

Reeves, J., J. Chen, X. L. Wang, R. Lund, and Q. Lu, 2007: A review and comparison of changepoint detection techniques for climate data. *J. Appl. Meteor. Climatol.*, **46**, 900–915, doi:10.1175/JAM2493.1.

Robinson, P. J., 2001: On the definition of a heat wave. *J. Appl. Meteor.*, **40**, 762–775, doi:10.1175/1520-0450(2001)040<0762:OTDOAH>2.0.CO;2.

Rohatgi, V. K., 1976: *An Introduction to Probability Theory and Mathematical Statistics.* John Wiley and Sons, 684 pp.

Rothfusz, L. P., 1990: The heat index ''equation'' (or, more than you ever wanted to know about heat index). NWS Tech. Attachment SR 90-23, 2 pp., https://www.weather.gov/media/ffc/ta_htindx.PDF.

Steadman, R. G., 1979: The assessment of sultriness. Part I: A temperature-humidity index based on human physiology and clothing science. *J. Appl. Meteor.*, **18**, 861–873, doi:10.1175/1520-0450(1979)018<0861:TAOSPI>2.0.CO;2.

Trenberth, K. E., and Coauthors, 2007: Observations: Surface and atmospheric climate change. *Climate Change 2007: The Physical Science Basis*, S. Solomon et al., Eds., Cambridge University Press, 235–336.

Ultsch, A., and F. Roske, 2002: Self-organizing feature maps predicting sea levels. *Inf. Sci.*, **144**, 91–125, doi:10.1016/S0020-0255(02)00203-7.

Wang, X.Y., and Coauthors, 2012: The impact of heatwaves on mortality and emergency hospital admissions from non-external causes in Brisbane, Australia. *Occup. Environ. Med.*, **69**, doi:10.1136/oem.2010.062141.

Yip, Z. K. and M. K. Yau, 2012: Application of artificial neural networks on North Atlantic tropical cyclogenesis potential index in climate change. *J. Atmos. Oceanic Technol.*, **29**, 1202–1220, https://doi.org/10.1175/JTECH-D-11-00178.1.

Zaman, M., G. Fang, K. Mehmood, and M. Saifullah, 2015: Trend change study of climate variables in Xin'anjiang-Fuchunjiang Watershed, China. *Adv. Meteor.*, **2015**, 507936, doi:10.1155/2015/507936.